10652 *Inorg. Chem.* **2009**, *48*, 10652–10657
DOI: 10.1021/ic901285f

Inorganic Chemistry
Article

Theoretical Study of the Pseudo-Jahn−Teller Effect in the Edge-Sharing Bioctahedral Complex $Mo_2(DXylF)_2(O_2CCH_3)_2(\mu_2\text{-}O)_2$

Justyna M. Żurek and Martin J. Paterson*

School of Engineering and Physical Sciences, Heriot-Watt University, Edinburgh, Scotland, EH14 4AS

Received July 3, 2009

A study of the D_{2h} to C_{2h} pseudo-Jahn−Teller distortion in the edge-sharing bioctahedral complex $Mo_2(DXylF)_2(O_2CCH_3)_2(\mu_2\text{-}O)_2$ is presented. We have performed extensive density functional theory (DFT) and complete active space self-consistent field (CASSCF) calculations. For both the full target complex and a model derived by replacing xylyl and methyl groups with hydrogens we observe that the central $Mo_2(\mu_2\text{-}O)_2$ motif displays C_{2h} rather than D_{2h} symmetry. Analytical CASSCF frequency calculations prove that the rhomboidal distortion of the complex from D_{2h} to C_{2h} is due to a vibronic mixing of the ground electronic state and a low-lying $\pi\delta^*$ excited state.

Introduction

The edge-sharing bioctahedral (ESBO) complexes exhibit a variety of molecular structures.[1−3] Their central motif with general formula $M_2(\mu_2\text{-}X)_2$, where M is a metal and X is a bridging-ligand (Figure 1), display a range of different M−M and M−X distances and different XMX and MXM angles depending on the oxidation state of the metal atom and the type of bridging ligand.[4−7]

Metal−metal bonding occurs by overlap of the *d*-orbitals on each metal center. Figure 2 shows the σ, σ^*, π, π^*, δ, and δ^* interactions between pairs of d-orbitals on each metal atom (M and M′) in the $Mo_2(DXylF)_2(O_2CCH_3)_2(\mu_2\text{-}O)_2$ complex. The energetic ordering is not straightforward with regards to the δ and δ^* orbitals. For example, it has been reported that different ESBO complexes can sometimes have the antibonding orbital lower-lying than the bonding one.[2,3,8] Whether the order is $\delta < \delta^*$ or $\delta > \delta^*$ depends significantly on the identity of the bridging atoms and their interactions with the pure metal centered orbitals.

We present computational studies on the structure of the $Mo_2(DXylF)_2(O_2CCH_3)_2(\mu_2\text{-}O)_2$ ESBO complex which was experimentally observed as having the shortest Mo−Mo double bond and displays a rhomboidal (C_{2h}) structure, rather than a square (D_{2h}) one at the central $Mo_2(\mu_2\text{-}O)_2$ motif.[9] Cotton et al. have suggested that the distortion from the ideal D_{2h} structure is caused by the pseudo-Jahn−Teller (pJT) effect resulting in a mixing of the ground electronic state with a low-lying excited state giving rise to a lower energy structure of C_{2h} symmetry.

The pJT effect is understood as a vibronic coupling between a pair of adiabatic electronic states (as obtained in the clamped nucleus Born−Oppenheimer approximation[10]). We note here that there is an unfortunate ambiguous terminology in the literature regarding the pseudo-Jahn−Teller effect. In the field of structural chemistry, one often finds the term "second-order Jahn−Teller" used interchangeably with pseudo-Jahn−Teller.[11−13] In the field of nonadiabatic chemistry this term has the more well-defined meaning of the coupling of the components of a degenerate electronic state via vibrational motion computed at second-order, that is, true Jahn−Teller coupling but at second order.[10,14] Below we follow this latter nomenclature and will continue to talk about pseudo-Jahn−Teller coupling to mean the vibronic coupling between nondegenerate electronic states via nondegenerate, nontotally symmetric vibrational motion. The importance of the pJT effect in structural chemistry is that it can be thought of as a mixing of the ground state potential energy surface with that of a nearby excited state along a nontotally symmetric normal vibrational coordinate (Figure 3), thereby changing the curvature of the ground state surface and lowering the energy of critical points.[15]

*To whom correspondence should be addressed. E-mail: m.j.paterson@hw.ac.uk.

(1) Cotton, F. A.; Walton, R. A. *Multiple Bonds Between Metal Atoms*; Clarendon Press: Oxford, 1993.
(2) Cotton, F. A.; Wilkinson, G.; Murillo, C. A.; Bochmann, M. *Advanced Inorganic Chemistry*, 6th ed.; Wiley-Interscience: New York, 1999.
(3) Shaik, S.; Hoffmann, R.; Fisel, C. R.; Summerville, R. H. *J. Am. Chem. Soc.* **1980**, *102*, 4555–4572.
(4) Cotton, F. A. *Polyhedron* **1987**, *6*, 667.
(5) Palacios, A. A.; Aullon, G.; Alemany, P.; Alvarez, S. *Inorg. Chem.* **2000**, *39*, 3166–3175.
(6) McGrady, J. E.; Stranger, R.; Lovell, T. *Inorg. Chem.* **1998**, *37*, 3802–3808.
(7) Canich, J. A. M.; Cotton, F. A.; Daniels, L. M.; Lewis, D. B. *Inorg. Chem.* **1987**, *26*, 4046–4050.
(8) Anderson, L. B.; Cotton, F. A.; DeMarco, D.; Fang, A.; Ilsley, W. H.; Kolthammer, B. W. S.; Walton, R. A. *J. Am. Chem. Soc.* **1981**, *103*, 5078–5086.
(9) Cotton, F. A.; Daniels, L. M.; Murillo, C. A.; Slaton, J. G. *J. Am. Chem. Soc.* **2002**, *124*, 2878–2879.
(10) Worth, G. A.; Cederbaum, L. S. *Annu. Rev. Phys. Chem.* **2004**, *55*, 127–158.
(11) Burdett, J. K. *Inorg. Chem.* **1981**, *20*, 1959–1962.
(12) Toyota, A.; Koseki, S. *J. Phys. Chem.* **1996**, *100*, 2100–2106.
(13) Cotton, F. A.; Donahue, J. P.; Hall, M. B.; Murillo, C. A.; Villagran, D. *Inorg. Chem.* **2004**, *43*, 6954–6964.
(14) Paterson, M. J.; Bearpark, M. J.; Robb, M. A.; Blancafort, L.; Worth, G. A. *Phys. Chem. Chem. Phys.* **2005**, *7*, 2100–2115.

Published on Web 10/15/2009

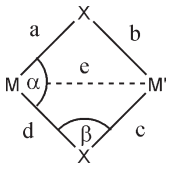

Figure 1. Geometrical parameters of the central $M_2(\mu_2\text{-}X)_2$ motif of an edge-sharing bioctahedral (ESBO) complex.

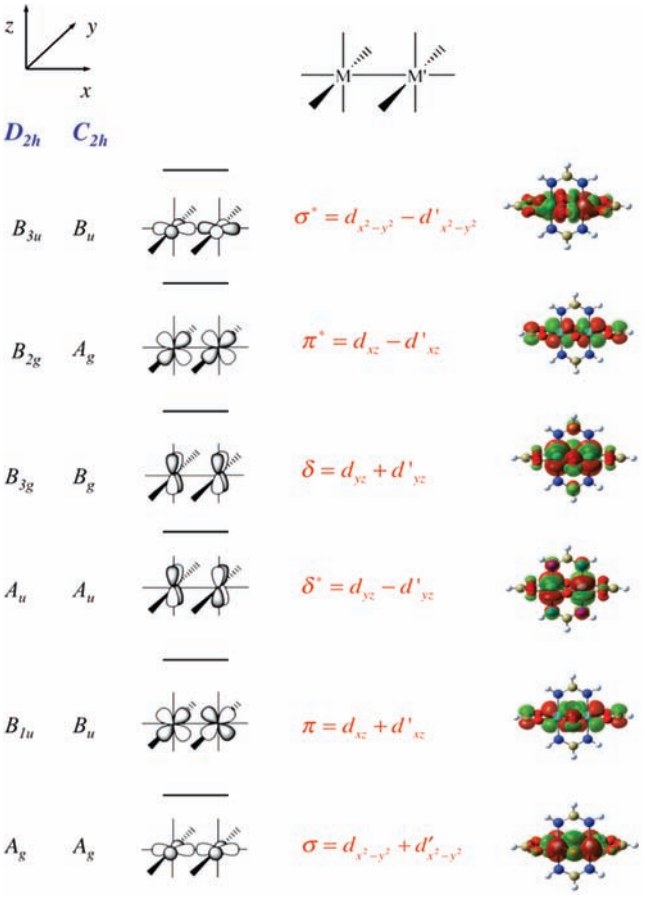

Figure 2. Primary orbitals involved in multiple metal−metal bonding in ESBO complexes. Schematic interactions between metal (M and M′) centers shown on the left side, optimized CASSCF orbitals shown on the right side.

Pearson provided the first detailed study of the pJT effect and developed a perturbative expansion of the ground state adiabatic potential energy surface in terms of displacements along normal coordinates Q_i.[16,17] The Pearson expansion is given below

$$E(Q_i) = E_0 + Q_i\left\langle \Psi_0 \left| \frac{\partial V}{\partial Q_i} \right| \Psi_0 \right\rangle + \frac{{Q_i}^2}{2}\left\langle \Psi_0 \left| \frac{\partial^2 V}{\partial^2 Q_i} \right| \Psi_0 \right\rangle + {Q_i}^2 \sum_j \frac{\left[\left\langle \Psi_0 \left| \frac{\partial V}{\partial Q_i} \right| \Psi_j \right\rangle\right]^2}{E_0 - E_j} + \ldots \quad (1)$$

(15) Bersuker, I. B. *Chem. Rev.* **2001**, *101*, 1067–1114.
(16) Pearson, R. G. *J. Am. Chem. Soc.* **1969**, *91*, 1252–1254.
(17) Pearson, R. G. *Proc. Natl. Acad. Sci. U.S.A.* **1975**, *72*, 2104–2106.

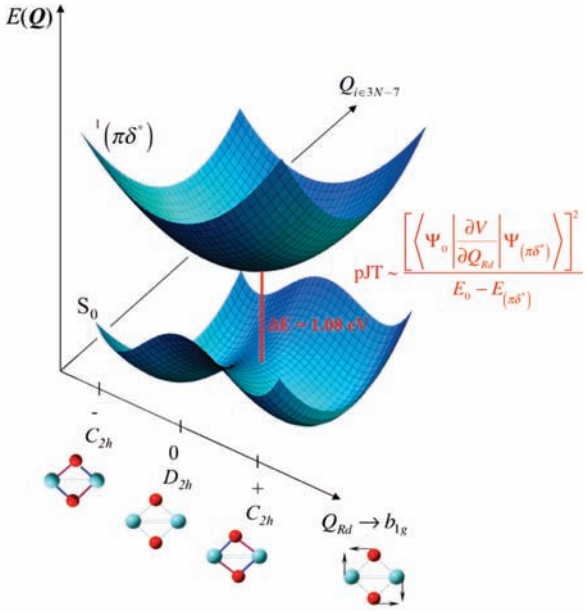

Figure 3. Schematic potential energy surfaces of the ground electronic state (S_0), and first excited singlet state ($S_1 - {}^1(\pi\delta^*)$) of the $Mo_2(DXylF)_2(O_2CCH_3)_2(\mu_2\text{-}O)_2$ complex. The rhomboidal distortion normal coordinate (Q_{Rd}) of b_{1g} symmetry is shown. Pseudo-Jahn−Teller coupling between the two electronic states gives the lower potential energy surface negative curvature along this coordinate, leading to equivalent minima of C_{2h} symmetry (equivalent Mo−O bonds are colored blue and purple) in the positive and negative distortions along Q_{Rd}.

where E is the electronic ground state energy, E_0 is the energy at the expansion point (the high symmetry structure), V is the nuclear−nuclear and nuclear−electronic terms of the potential energy in the Hamiltonian, E_j is the energy of the jth excited electronic state, and Ψ_0 is the ground state electronic wave function, while Ψ_j is that of excited electronic states. There is an expansion along each of the $3N - 6$ normal vibrational coordinates $Q_{i\in 3N-6}$.

The first order term is always zero because the gradient of the optimized molecular structure is zero, that is, in the terminology of Bersuker et al. the structure is force equilibrated.[18] The relative magnitude of both quadratic terms determines if the pJT coupling lowers the symmetry of the optimized structure.[19] The first quadratic term is always positive for an optimized molecular geometry, although the proof of this is far from trivial (see ref 18. and references therein). Bersuker and co-workers have proved this for Hartree−Fock and configuration interaction electronic wave functions.[20] The second quadratic term is always negative, since the excited state energies E_j are higher than the ground state energy (i.e., $E_0 < E_j$). This second quadratic term is the pJT coupling term and allows electronic states to mix via nonsymmetric vibrations (this term accounts for relaxation of the wave function at distorted geometries). Thus, whether the ground state energy rises or is lowered along the direction Q_i depends upon the relative magnitude of both of these terms. Finally we note that although eq 1 above is very useful for illustrative purposes, more rigorous nonperturbative

(18) Bersuker, I. B. *The Jahn-Teller Effect*; Cambridge University Press: New York, 2006.
(19) Bearpark, M. J.; Blancafort, L.; Robb, M. A. *Mol. Phys.* **2002**, *100*, 1735–1739.
(20) Bersuker, I. B.; Balabanov, N. B.; Pekker, D.; Boggs, J. E. *J. Chem. Phys.* **2002**, *117*, 10478–10486.

treatments of the pJT effect have been developed,[18,21] and in fact this body of work has shown that the pJT effect is the only source of configurational instability in molecules in nondegenerate electronic states.

Symmetry informs which of these symmetry adapted normal vibrations (Q_i) give rise to zero change in the energy at second-order. For example, the matrix elements in eq 1 above are nonzero only when the direct product of the irreducible representations (Γ) of each symmetry species contains the totally symmetric irreducible representation of the molecular point group (Γ_{TS}). In the final term,

$$\left\langle \Psi_0 \left| \frac{\partial V}{\partial Q_i} \right| \Psi_j \right\rangle \neq 0 \quad \text{if} \quad \Gamma_{\Psi_0} \otimes \Gamma_{Q_i} \otimes \Gamma_{\Psi_j} \supset \Gamma_{TS} \qquad (2)$$

Thus, a nontotally symmetric distortion that lowers the energy in a closed shell electronic ground state (Γ_{TS}) must have the same symmetry as that of the excited electronic state involved in the vibronic coupling.

It has until recently been assumed that the energy difference denominator in the final quadratic term in eq 1 meant that only low-lying excited electronic states could give rise to pJT distortions; however, recent work has shown that even states quite high in the electronic manifold can overcome the energetic penalty due to very large vibronic coupling matrix elements (eq 2).[15,18,21,22] Previous work in assigning a pJT effect has relied upon showing that low-lying electronic states of the correct symmetry exist and that the potential energy surface has negative curvature along vibrational coordinates of the appropriate symmetry.[23]

Over the years the pJT effect has become very important in structural chemistry. It has been used to successfully explain many diverse chemical phenomena including molecular structure, molecular fluxionality, and electron delocalization in mixed valence compounds.[18] Inorganic chemistry is a rich source of such phenomena,[11,15,18,21] from relatively small molecules,[24,25] to many large transition metal complexes,[26,27] to the solid state.[9,28,29]

In this article we present an examination of pJT effect in the $Mo_2(DXylF)_2(O_2CCH_3)_2(\mu_2\text{-}O)_2$ complex using a Complete Active Space Self-Consistent Field (CASSCF) Hessian matrix test originally proposed by Bearpark et al.[19] The Hessian is the matrix containing the second derivatives of the electronic energy with respect to nuclear coordinates and can be evaluated analytically by differentiating the appropriate energy expression. The desirable feature of the CASSCF symmetry-constrained Hessian method is that it conclusively demonstrates a vibronic coupling between electronic states and therefore is capable of showing that a nonsymmetric distortion is entirely electronic in origin. The coupling is thus proved to be responsible for the distorted lower symmetry structure, rather than assumed due to, for example, small energy differences between electronic states. Proving that an electronic induced distortion exists in an isolated molecule is of importance for the solid state also, showing that any observed distortion in the crystal structure is not (entirely) due to crystal packing.

The method relies on analytical CASSCF Hessian calculations. If the CASSCF wave function is constructed by restricting the configuration state functions (CSFs) to functions of a particular symmetry class, then pJT coupling (eq 1) is automatically precluded if that symmetry class does not contain the coupled states in eq 1. The Hamiltonian matrix is block diagonal in a basis of symmetry adapted CSFs, so CSFs of a different symmetry do not contribute to the energy of a given state. Likewise for a nondegenerate state the gradient vector is totally symmetric, and geometry optimization only requires CSFs with the same symmetry as the state of interest. However, at second-order CSFs of different symmetries can mix under a nuclear perturbation. In calculating CASSCF second derivatives the coupled-perturbed multiconfiguration self-consistent-field (CP-MCSCF) equations are solved, and these include both orbital mixing and configuration mixing (the so-called derivative coupling contributions).[30] The derivative coupling terms represent the real mixing of electronic states under a nuclear perturbation,[19] and the presence of these terms in the CP-MCSCF equations can be controlled via symmetry constraints. If separate CASSCF calculations using different symmetry restrictions are performed (e.g., building the CASSCF wave function from the set of CSFs spanning all irreducible representations of the point group vs building the CASSCF wave function from the set of CSFs spanning only the irreducible representation of the ground electronic state), then the pJT effect is manifest in a change of curvature for a particular nontotally symmetric normal coordinate (i.e., a change from real to imaginary vibrational frequency) when the vibronically coupled state is included in the calculation of the perturbed wave function.

This method has been used successfully in several studies and has been used to explain the structures of both closed- and open-shell organic molecules such as pentalene, cyclobutadiene, and cyclohexane.[14,19,31] We have recently used this method to explain the pseudorotation barrier in singlet $Cr(CO)_5$ as arising from a pJT coupling (as opposed to true second-order Jahn−Teller coupling) between the closed shell ground state and a metal-centered ligand-field excited state.[27] This result confirmed previous conclusions obtained in trying to fit a model vibronic coupling Hamiltonian for the $Cr(CO)_5$ system, used to perform wavepacket dynamics simulations of the ultrafast electronic relaxation.[32]

As discussed above, the pJT effect has been of prime importance in the field of structural inorganic chemistry,

(21) Bersuker, I. B. *J. Mol. Struct.* **2007**, *838*, 44–52.
(22) Garcia-Fernandez, P.; Bersuker, I. B.; Boggs, J. E. *J. Chem. Phys.* **2006**, *125*, 104102.
(23) Paterson, M. J.; Chatterton, N. P.; McGrady, G. S. *New J. Chem.* **2004**, *28*, 1434–1436.
(24) Garcia-Fernandez, P.; Bersuker, I. B.; Boggs, J. E. *J. Phys. Chem.* **2007**, *111*, 10409–10415.
(25) Viel, A.; Eisfeld, W.; Neumann, S.; Domcke, W.; Manthe, U. *J. Chem. Phys.* **2006**, *124*, 214306.
(26) Borshch, S. A.; Ogurtsov, I. Y.; Bersuker, I. B. *J. Struct. Chem.* **1982**, *23*, 825–829.
(27) McKinlay, R. G.; Paterson, M. J. The Jahn-Teller Effect in Binary Transition Metal Carbonyl Complexes. In *The Jahn-Teller Effect: Fundamentals and Implications for Physics and Chemistry*; Springer Series in Chemical Physics; Köppel, H., Barentzen, H., Yarkony, D. R., Eds.; Springer-Verlag: Heidelberg, 2010 in press.
(28) Aguado, F.; Rodriguez, F.; Valiente, R.; Itie, J. P.; Munsch, P. *Phys. Rev. B* **2004**, 70.
(29) Koppitz, J.; Schrimer, O. F.; Seal, M. *J. Phys. C. Solid State Phys.* **1986**, *19*, 1123–1133.
(30) Yamamoto, N.; Vreven, T.; Robb, M. A.; Frisch, M. J.; Schlegel, H. B. *Chem. Phys. Lett.* **1996**, *250*, 373–378.
(31) Blancafort, L.; Bearpark, M. J.; Robb, M. A. *Mol. Phys.* **2006**, *104*, 2007–2010.
(32) Worth, G. A.; Welch, G.; Paterson, M. J. *Mol. Phys.* **2006**, *104*, 1095–1105.

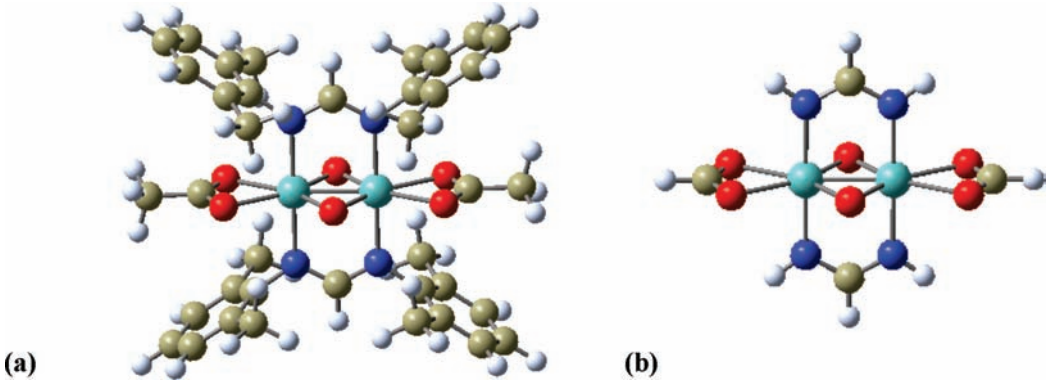

Figure 4. Structures of the $Mo_2(DXylF)_2(O_2CCH_3)_2(\mu_2\text{-}O)_2$ complex: (a) optimized target system taken from crystal structure in ref 9 and (b) model complex used in multiconfiguration calculations of pseudo-Jahn−Teller vibronic coupling.

and this represents quite a challenge for multiconfigurational wave functional methods. The system studied here, a large transition bimetal complex, is such a system. We have thus developed a model of the full target system shown in Figure 4 below. Although the primary objective in this paper is to explain the pJT effect in the model using CASSCF, we have additionally undertaken extensive density functional theory (DFT) calculations on both the target (Figure 4a) and model (Figure 4b) systems.

Computational Details

DFT calculations were performed on the target system starting from the crystal structure in ref 9 and a model system (in which xylyl and methyl groups were substituted with hydrogens) using a range of standard functionals in conjunction with the SDD effective core potential basis set on the molybdenum atoms, and the 6-311G** basis set for nitrogen, oxygen, carbon, and hydrogen atoms. The exchange correlation functional was found to have minimal effect, and so only the B3LYP results are quoted below. CASSCF calculations were performed using a hierarchy of active spaces: a basic active space consisted of four electrons distributed among the σ, π, and δ bonding orbitals, and their correlating σ^*, π^*, and δ^* antibonding orbitals (shown in Figure 2). This active space was used for geometry optimization, and analytical frequency calculation. Single-point CASSCF calculations were also performed using augmented active spaces obtained by adding in-plane metal−oxygen bonding and antibonding orbitals: two different (6,8) active spaces and a (8,10) active space. For the CASSCF geometry optimization and frequency calculations the 3-21G* basis was used on the molybdenums, with the STO-3G basis on all other atoms, while for the single-point calculations the same basis as discussed above for DFT was used. We note that the general features of the ground state CASSCF wave function were found to be insensitive to the one-electron basis set used. All computations were performed using the Gaussian 03 program[33] on a Linux cluster with Intel Xeon Harpertown processors.

Results and Discussion

The framework of the $Mo_2(DXylF)_2(O_2CCH_3)_2(\mu_2\text{-}O)_2$ complex is very interesting due to the shortest metal−metal distances among all the Mo(IV) ESBO complexes.[9] To understand its structure we performed a series of DFT optimizations on the target and model systems. The starting geometry of the target was taken as the crystal structure from ref 9. The optimized geometrical parameters for the central $Mo_2(\mu_2\text{-}O)_2$ motif are given in Table 1. For the large target system the difference between nonequivalent bondlengths (a and b, c and d in Figure 1) is quite small, but nevertheless it is nonzero and shows that the central motif adopts a C_{2h} geometry. The ordering of the Kohn−Sham orbitals here reflects previous work in that the δ^* orbital is the lowest unoccupied molecular orbital (LUMO) and lies below the δ orbital (the LUMO + 1); the highest occupied molecular orbital (HOMO) is the π-bonding orbital.

The distortion in the model system is more pronounced and closer to the experimental difference. The rhomboidal distortion vibrational frequency (ν_{Rd}) is 47.91 i cm^{-1} for geometries optimized under D_{2h} constraints, which becomes 23.34 cm^{-1} at the true C_{2h} minimum. The Kohn−Sham orbital ordering has the π^* orbital as the LUMO, although it is almost degenerate with the δ^* orbital, which again lies below the δ orbital.

Time-dependent density functional theory (TD-DFT) calculations were also performed to determine the nature and energy of the lowest lying singlet electronic state. The results of the TD-B3LYP calculations are given in Table 2. For the target system the first singlet excited state (a^1B_{1g}) has a dominant particle−hole configuration involving an electron transferred from the HOMO to the LUMO, that is, from the π-bonding to the δ-antibonding orbital. Likewise for the model system the first excited state is $^1(\pi\delta)$, corresponding to HOMO → LUMO + 1. The energy gaps for the model and target systems are quite close (1.280 vs 1.251) at the C_{2h} minima. The energy gap for the model at the constrained D_{2h} geometry is lower at 1.266 eV as is expected in a pJT situation (see for example Figure 3). The next state of B_{1g} symmetry of the model is at 4.292 eV. We note that the S_1 (a^1B_{1g}) state is not optically bright via a one-photon transition by virtue of symmetry selection rules.

(33) Frisch, M. J.; Trucks, G. W.; Schlegel, H. B.; Scuseria, G. E.; Robb, M. A.; Cheeseman, J. R.; Montgomery, J., J. A.; Vreven, T.; Kudin, K. N.; Burant, J. C.; Millam, J. M.; Iyengar, S. S.; Tomasi, J.; Barone, V.; Mennucci, B.; Cossi, M.; Scalmani, G.; Rega, N.; Petersson, G. A.; Nakatsuji, H.; Hada, M.; Ehara, M.; Toyota, K.; Fukuda, R.; Hasegawa, J.; Ishida, M.; Nakajima, T.; Honda, Y.; Kitao, O.; Nakai, H.; Klene, M.; Li, X.; Knox, J. E.; Hratchian, H. P.; Cross, J. B.; Bakken, V.; Adamo, C.; Jaramillo, J.; Gomperts, R.; Stratmann, R. E.; Yazyev, O.; Austin, A. J.; Cammi, R.; Pomelli, C.; Ochterski, J. W.; Ayala, P. Y.; Morokuma, K.; Voth, G. A.; Salvador, P.; Dannenberg, J. J.; Zakrzewski, V. G.; Dapprich, S.; Daniels, A. D.; Strain, M. C.; Farkas, O.; Malick, D. K.; Rabuck, A. D.; Raghavachari, K.; Foresman, J. B.; Ortiz, J. V.; Cui, Q.; Baboul, A. G.; Clifford, S.; Cioslowski, J.; Stefanov, B. B.; Liu, G.; Liashenko, A.; Piskorz, P.; Komaromi, I.; Martin, R. L.; Fox, D. J.; Keith, T.; Al-Laham, M. A.; Peng, C. Y.; Nanayakkara, A.; Challacombe, M.; Gill, P. M. W.; Johnson, B.; Chen, W.; Wong, M. W.; Gonzalez, C.; Pople, J. A. *Gaussian 03*, Revision D.01; Gaussian, Inc.: Wallingford, CT, 2004.

Table 1. Optimized Geometrical Parameters of $Mo_2(\mu_2\text{-}O)_2$ Motif: Bond Lengths (a−e), Angles (α, β), and Rhomboidal Vibrational Frequency (ν_{Rd}) (corresponding to $D_{2h}-C_{2h}$ distortion)

$Mo_2(\mu_2\text{-}O)_2$ motif point group	optimized geometrical parameters						
	a, c (Å)	b, d (Å)	Δab = Δcd (Å)	e (Å)	α (deg)	β (deg)	ν_{Rd}[d] (cm^{-1})
			B3LYP[a]				
			Target				
C_{2h}	1.961	1.964	0.003	2.329	107.2	72.8	55.06
			Model				
D_{2h}	1.957	1.957	0.000	2.329	107.0	73.0	47.91 *i*
C_{2h}	1.974	1.941	0.033	2.330	107.0	73.0	23.34
			CAS(4,6)[a]				
D_{2h}	1.933	1.933	0.000	2.553	97.4	82.7	
C_{2h}	1.860	2.004	0.144	2.765	88.7	91.3	
			CAS(4,6)[b]				
D_{2h}	1.910	1.910	0.000	2.527	97.2	82.9	452.91 *i*
C_{2h}	1.760	2.087	0.327	2.542	97.7	82.3	156.61
			Experiment[c]				
C_{2h}	1.960	1.913	0.047	2.306	107.0	73.0	

[a] SDD basis on Mo; 6-311G** basis on C, N, O, and H. [b] 3-21G* basis on Mo; STO-3G basis on C, N, O, and H. [c] Reference 9. [d] $i = \sqrt{(-1)}$.

Table 2. Comparison of Vertical Excitation Energies of the S_1 $^1(\pi\delta^*)$ State for the Model (ΔE_M) and Target Systems (ΔE_T) Using Time-Dependent Density Functional Theory (B3LYP exchange correlation functional) and CASSCF[a]

method	ΔE_T (eV)		ΔE_M (eV)	
	D_{2h}	C_{2h}	D_{2h}	C_{2h}
TD-B3LYP		1.251	1.266	1.280
CAS(4,6)			1.084	
CAS(6,8)			1.544	
CAS(8,10)			1.671	

[a] All calculations reported here used the SDD effective core potential on Mo and the 6-311G** basis on N, O, C, and H.

Our final point regarding DFT is that the pJT effect is one area where DFT has some inherent problems due to the single-configurational nature of the underlying Kohn−Sham state. Static correlation effects are poorly described in DFT, and as the CASSCF results below show, the model system studied here exhibits a fair degree of this. However, since the electronic state is closed-shell across the ground adiabatic potential energy surface, DFT can probably be used with caution.

Turning now to the CASSCF calculations, the ground electronic state (S_0) is ^1A_g, and the first thing to note is the orbital occupations shown in Table 3. These are the diagonal elements of the one-electron density matrix and give an indication about the multiconfigurational nature of the wave function. For all of the active spaces detailed in Table 2 it is clear that the electronic structure is slightly more complicated than just $\sigma^2\pi^2$ as would be imposed in a single-configuration calculation. We observe significant correlation between electrons in the σ-bonding and σ-antibonding orbitals and electrons in the π-bonding and π-antibonding orbitals: indicated by the significant population of the antibonding orbitals. The larger active spaces obtained by adding in-plane M−O orbitals (denoted by the largest O centered component in Table 3) do not qualitatively change the nature of the wave function. We also note that the CASSCF density of S_0 in the various active spaces changes very little with the quality of basis set, giving us confidence that the smaller basis used in the analytical frequency calculations (vide infra) generates accurate CASSCF wave functions.

The first excited state S_1 clearly involves the transfer of electron density from the π-system to the δ-system. S_1 can therefore be identified as the $^1(\pi\delta^*)$ state, and again there is significant correlation between electrons in the δ and δ^* orbitals. The CASSCF state based results confirm the idea of δ and δ^* ordering as in the S_1 state the occupation of the δ^* orbital is significantly greater than that of the δ orbital; that is, the electronic structure of the S_1 state can be approximated as $\sigma^2\pi^1\delta^{*1}$, although again there is significant correlation in the σ, π, and δ systems.

We now turn to the CASSCF frequency analysis of the pJT effect causing the $D_{2h}-C_{2h}$ distortion of the central pattern in this complex. The CAS(4,6) optimized geometrical parameters for both the D_{2h} and C_{2h} structures are given in Table 1. Analytical frequency calculations using a CASSCF wave function expanded in a basis of all the CSFs (total = 105) confirms that the D_{2h} structure is a transition state. The transition vector is the rhomboidal distortion coordinate (Q_{Rd}) and has b_{1g} symmetry, with a vibrational frequency of 452.91 *i* cm^{-1}. This transition vector is shown schematically in Figure 3 for the central $Mo_2(\mu_2\text{-}O)_2$ motif. When we restrict the frequency calculation to include CSFs of only the ground state symmetry A_g (total = 21), this vibrational frequency is no longer imaginary (37.70 cm^{-1}). We can conclude here that there is a vibronic coupling between the ground electronic state ($S_0 = {}^1A_g$) and the first excited state ($S_1 = {}^1B_{1g} = {}^1(\pi\delta^*)$). The symmetries of the various entities are given in eq 3. The CASSCF energy gap between the two electronic states is 0.947 eV (Table 2). Thus, the fact that the curvature along the rhomboidal distortion mode changes when CSFs of B_{1g} symmetry are included in the frequency

Table 3. Orbital Occupations Obtained as the Diagonal Elements of the CASSCF One-Electron Density Matrix for the S_0 and S_1 States[a]

	orbital occupation									
state	O sp_x	O sp_y	σ	π	δ^*	δ	π^*	σ^*	O sp_x*	O sp_y*
					CAS(4,6)					
S_0			1.732	1.301	0.001	0.001	0.699	0.266		
S_1			1.722	0.650	0.648	0.351	0.353	0.276		
					CAS(6,8)					
S_0		1.999	1.873	1.701	0.001	0.002	0.299	0.123		0.000
S_1		1.999	1.865	0.783	0.781	0.220	0.218	0.133		0.000
					CAS(6,8)					
S_0	1.962		1.879	1.723	0.021	0.019	0.278	0.117	0.000	
S_1	1.804		1.876	0.929	0.912	0.191	0.167	0.121	0.000	
					CAS(8,10)					
S_0	1.974	1.968	1.887	1.730	0.003	0.004	0.269	0.113	0.029	0.023
S_1	1.970	1.977	1.881	0.806	0.803	0.200	0.196	0.119	0.027	0.022

[a] In addition to the basic (4,6) active space shown in Figure 2, augmented active spaces including bonding and anti-bonding oxygen centred orbitals were also investigated. All calculations reported here used SDD effective core potential on Mo and the 6-311G** basis on N, O, C, and H.

calculation indicates that a pJT coupling operates (eq 2 is fulfilled). CASSCF calculations also confirm that the S_1 $^1(\pi\delta^*)$ state has its minimum energy geometry at a D_{2h} structure (Figure 1).

$$\begin{aligned} &\Psi_0 \rightarrow {}^1A_g \\ &Q_{Rd} \rightarrow b_{1g} \\ &\Psi_j = {}^1(\pi\delta^*) \rightarrow {}^1B_{1g} \\ &\Gamma_{\Psi_0} \otimes \Gamma_{Q_{Rd}} \otimes \Gamma_{\Psi_i} \supset A_g \end{aligned} \tag{3}$$

Conclusions

We have studied the pseudo-Jahn−Teller effect in the edge-sharing bioctahedral complex $Mo_2(DXylF)_2(O_2CCH_3)_2(\mu_2\text{-}O)_2$ using a variety of computational techniques. Our results show that in both the large target, and a smaller model system, the central $Mo_2(\mu_2\text{-}O)_2$ motif has a rhomboidal shape and C_{2h} symmetry. CASSCF calculations reveal that the distortion from D_{2h} to C_{2h} symmetry is caused by a vibronic coupling between the ground electronic state and the first excited singlet state, which can be characterized as a $^1(\pi\delta^*)$ state.

Acknowledgment. We thank the EPSRC for funding through Grant EP/F01709X.

Supporting Information Available: Cartesian coordinates of all optimized geometries. This material is available free of charge via the Internet at http://pubs.acs.org.